THE JOURNAL OF PHYSICAL CHEMISTRY B

Article

pubs.acs.org/JPCB

Terms of Use

Factors That Drive Peptide Assembly from Native to Amyloid Structures: Experimental and Theoretical Analysis of [Leu-5]-Enkephalin Mutants

Thanh D. Do,[⊥,†] Nichole E. LaPointe,[⊥,‡] Smriti Sangwan,[⊥,§] David B. Teplow,[∥] Stuart C. Feinstein,[‡] Michael R. Sawaya,[§] David S. Eisenberg,[§] and Michael T. Bowers*[,†]

[†]Department of Chemistry and Biochemistry and [‡]Neuroscience Research Institute and Department of Molecular, Cellular and Developmental Biology, University of California, Santa Barbara, California 93106, United States

[§]Departments of Chemistry and Biochemistry and Biological Chemistry, Howard Hughes Medical Institute, UCLA-DOE Institute for Genomics and Proteomics, and [∥]Department of Neurology, David Geffen School of Medicine at UCLA, Mary S. Easton Center for Alzheimer's Disease Research at UCLA, and Brain Research Institute and Molecular Biology Institute, University of California, 635 Charles Young Drive South, Los Angeles, California 90095, United States

Supporting Information

ABSTRACT: Five different mutants of [Leu-5] Enkephalin YGGFL peptide have been investigated for fibril formation propensities. The early oligomer structures have been probed with a combination of ion-mobility mass spectrometry and computational modeling. The two peptides YVIFL and YVVFL form oligomers and amyloid-like fibrils. YVVFV shows an early stage oligomer distribution similar to those of the previous two, but amyloid-like aggregates are less abundant. Atomic resolution X-ray structures of YVVFV show two different modes of interactions at the dry interface between steric zippers and pairs of antiparallel β-sheets, but both are less favorable than the packing motif found in YVVFL. Both YVVFV and YVVFL can form a Class 6 steric zipper. However, in YVVFV, the strands between mating sheets are parallel to each other and in YVVFL they are antiparallel. The overall data highlight the importance of structurally characterizing high order oligomers within oligomerization pathways in studies of nanostructure assembly.

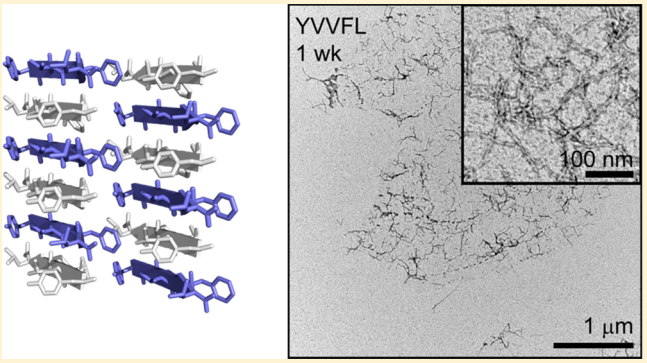

INTRODUCTION

The accumulation of cross-β-pleated aggregates and inclusions is a pathological hallmark in many diseases.[1−3] Converging experimental evidence suggests that sequence similarity in residue type (hydrophobic vs polar) patterning[4] and monomer conformations allow peptides to gain access to certain oligomeric (e.g., cylindrins,[5,6] out-of-register β-sheet,[7] ion-channel barrels[8,9]) and protofibrillar structures (e.g., steric zipper,[2,10,11] β-arcades[12]). Such assemblies are often driven by short fragments of the full-length sequence.[13,14] In addition, well-defined nanostructures formed by short peptide assemblies have recently emerged as a potential source of inexpensive functional materials.[15−18] Hence, one of the major objectives in the field of protein chemistry is to determine the driving forces behind the formation of ordered, multimeric structures. Small aggregating peptides and proteins accessible by both experiment and computation have provided powerful means to investigate at atomistic and oligomeric levels the subtle factors regulating aggregation propensity and morphology transitions. As a result, peptide models can be designed for an *ad hoc* target,[19−21] to satisfy a variety of physical and biological needs. Recent approaches focus on designing aggregating peptides *de novo* from combinatorial libraries,[19−21] in which the starting peptides are not limited by size and intrinsic properties (e.g., hydrophobicity and structural propensity).

Here, we attempt to identify mutations that can convert [Leu5]-Enkephalin (YGGFL), a pentapeptide neurotransmitter that binds to opiate receptors[22] and is known to form only globular aggregates,[14] into peptides that can aggregate to well-defined fibrils. We investigate the early stages of aggregation using ion mobility mass spectrometry (IM-MS) and compare the resulting experimental observations to temperature-based replica exchange molecular dynamics (T-REMD) simulations in explicit solvent. Transmission electron microscopy (TEM) and X-ray crystallography are utilized to examine the final morphologies and macroscopic structures of the mutant aggregates. We show that for pentapeptide systems with a high degree of sequence similarity, the aggregation behaviors

Received: March 11, 2014
Revised: June 8, 2014
Published: June 10, 2014

 © 2014 American Chemical Society dx.doi.org/10.1021/jp502473s | J. Phys. Chem. B 2014, 118, 7247−7256

(i.e., aggregating or nonaggregating), kinetics, and macroscopic morphologies are determined and regulated by inter-subunit interactions and their stabilities.

MATERIALS AND METHODS

Mutations of [Leu-5]-Enkephalin Using PASTA. We tested all possible single, double, and triple YGGFL mutants and computed amyloid structure aggregation (PASTA)[23,24] score for each peptide sequence. This approach is similar to one used in our previous study on NNQQNY mutants.[25] Because YGGFL is a nonaggregating peptide, at least two mutations are required to obtain a good PASTA score. The final list of the five mutants predicted to be most aggregating (i.e., yielding the most negative PASTA score) included YVVFV, YVIFL, YVVFL, YVVVL, and YVGVL (Table 1). On the basis of sequence similarity, we grouped the three peptides YVVFV, YVIFL, and YVVFL into Set I, and the remaining two, YVVVL and YVGVL, into Set II.

Table 1. Aggregation Propensity Scores for YGGFL and Its Mutants Obtained from the PASTA Method

sequence	PASTA score	remark
YGGFL (wt)	+0.03	non β-aggregating
YVVFV	−7.55	very high predicted β-aggregation propensity
YVIFL	−6.24	high sequence similarity to the wt and high predicted β-aggregation propensity
YVVFL	−6.30	high sequence similarity to the wt and high predicted β-aggregation propensity
YVVVL	−7.05	very high predicted β-aggregation propensity
YVGVL	−3.42	medium β-aggregation propensity

The five peptides were synthesized by FMOC (*N*-(9-fluorenyl)methoxycarbonyl) chemistry with free NH_2 and COOH termini. The peptides were purified by reversed-phase HPLC, and characterized by mass spectrometry and amino acid analysis to confirm peptide purity and integrity (>94% purity).

Ion Mobility Mass Spectrometry (IM-MS). Peptide stock solutions were prepared at 2.0 mg/mL in hexafluoro-2-propanol (TCI America) to disrupt oligomer formation and prevent aggregation. Aliquots of stock solutions were evaporated overnight before being diluted in water or 20 mM ammonium acetate buffer (pH = 7.0) to the final concentration of 200 μM.

IM-MS offers a versatile method to characterize mass-selected biomolecule ions in the gas phase where under carefully controlled conditions, solution phase structures can often be retained.[26] Specific oligomers can be separated and their structural information can be derived from experimental collision cross sections. In the experiments, ions were generated through the means of nano-ESI, stored in a source funnel and subsequently pulsed into a drift cell filled with He gas at high pressure. The ions drift through the cell with a constant velocity due to the effects of a weak electrical field and experience a drag force due to collisions with buffer gas molecules. Drift velocity can be related to the reduced ion mobility K_0, and used to calculate the experimental collision cross sections σ as follows:[27,28]

$$\sigma \approx \Omega_{avg} = \frac{(18\pi)^{1/2}}{16}\left[\frac{1}{m} + \frac{1}{m_b}\right]^{1/2} \frac{ze}{(k_B T)^{1/2}} \frac{1}{K_0} \frac{1}{N}$$

where m and m_b are the molecular weights of the ions and buffer gas molecules, respectively, ze is the charge of the ion, N is the buffer gas density and Ω_{avg} is the average collision cross section integral, which approximates the average collision cross section σ.

The IM-MS instrument was built in-house and consists of a nano-ESI source, an ion funnel, a 200 cm long drift cell and a quadrupole mass filter.[29]

Molecular Dynamics Simulations. Explicit solvent T-REMD simulations[30] for the tetramers of YGGFL, YVVFV, YVIFL, YVVVL, YVVFL, and YVGVL were performed using the GROMACS 4.5.3 package[31,32] and the all-atom Optimized Potentials for Liquid Simulations (OPLS-AA) force field[33,34] in TIP3P water[35] with periodic boundary condition. Simulation details can be found in Supporting Information section S2. The production run was 200 ns long per replica, but only the last 100 ns of data was subjected to analysis. The trajectories at 300 K were clustered using the Daura algorithm[36] to identify populated conformations.

Transmission Electron Microscopy. Prior to obtaining TEM data, 200 μM samples were incubated at room temperature for 3 days to 1 week under constant shaking. To prepare samples for TEM, peptides were fixed in glutaraldehyde (final glutaraldehyde concentration = 1.6%, from an 8% aqueous stock solution, Electron Microscopy Sciences) for 15 min at room temperature. A drop of the fixed sample was then absorbed for 1.5 min onto a 300-mesh Formvar/carbon coated copper grid (Electron Microscopy Sciences). Excess sample was wicked away, and the grid was rinsed with deionized water and then stained for 20 s with 2% uranyl acetate (Ted Pella, Inc.). Grids were viewed on a JEOL-1230 TEM microscope at 80 kV. Digital images were acquired using an ORCA camera and AMT Image Capture Software (Version 5.24, Woburn, MA, USA). Fiber measurements were performed manually using ImageJ (version 1.44p, US National Institutes of Health, Bethesda, MD, USA).

X-ray Crystallography. *Crystallization.* Out of the five mutants, only YVVFV and YVVFL were chosen for X-ray crystallography analysis, due to their similarity in sequences and early oligomer distributions but different aggregation behaviors (see next sections). Crystals of YVVFV and YVVFL were grown in hanging drop VDX plates (Hampton Research, Aliso Viejo, CA). Both peptides were dissolved in 10 mg/mL in water. The reservoir solution contained 0.1 M sodium cacodylate pH 6.5, 0.1 M magnesium acetate and 15% 2-methyl-2,4-pentanediol (MPD) for YVVFV, and 0.2 M potassium thiocyanante and 25% poly(ethylene glycol) (PEG) 3350 for YVVFL. Peptide and reservoir solutions were mixed in a 2:1 ratio by volume. Brick-like crystals of YVVFV appeared after 2−3 days at ambient temperature. The crystals were cryoprotected by quick dipping in a solution containing 60% reservoir and 40% MPD, then mounted in CrystalCap HT Cryoloops (Hampton Research, Aliso Viejo, CA) and flash cooled in a cryogenic nitrogen stream (100 K). Needle-like crystals of YVVFL appeared overnight and were mounted on glass capillaries.

Data Collection and Processing. All data was collected at the Advanced Photon Source (Chicago, IL) beamline 24-ID-E. A single crystal of YVVFV diffracted to 1.1 Å. Data indexing,

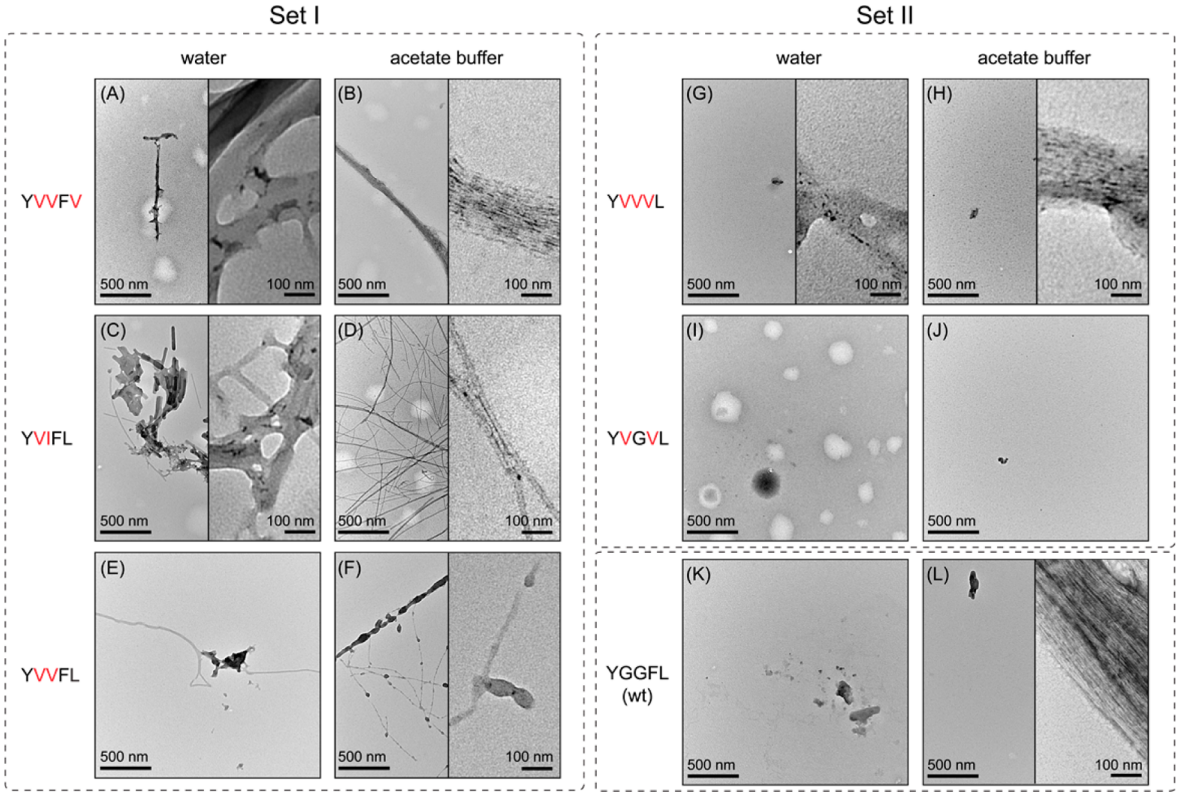

Figure 1. TEM images of peptides incubated for 1 week in water or 20 mM ammonium acetate buffer, pH 7 under constant shaking conditions. Lower magnification images show representative fields, and the higher magnification insets show the morphology of any aggregates present in the sample.

integration, and scaling were performed with XDS/XSCALE.[37] The structure was solved by direct methods using SHELXD. Crystals of YVVFL diffracted to 1.9 Å and the structure was solved by molecular replacement using PHASER.[38] Initial data indexing and integration was done by XDS[37] and DENZO.[39] Ideal antiparallel β-strands were used as search models. Model building and refining were performed with COOT[40] and PHENIX.[41]

RESULTS AND DISCUSSION

Transmission Electron Microscopy Shows Formation of Fibrillar Aggregates in Set I Peptides and YVVVL. Figure 1 shows representative TEM images of aggregates formed by the five peptides after 1 week of constant shaking in either buffer or water (Figure 1A–F). The insets in this figure show aggregates at higher magnification, although in some cases aggregates were rare (discussed below). In general, aggregation in buffer resulted in more well-defined fibrillar aggregates, whereas aggregates formed in water tended to have a "fused" or amorphous appearance. YVVFV showed rare, amorphous or fused aggregates in water (Figure 1A), and a few bundles of fibrillar aggregates in buffer (Figure 1B). In contrast, YVIFL showed a mixture of fibrillar and amorphous aggregates in water (Figure 1C), and abundant, well-defined fibers in buffer (Figure 1D) that were sometimes present as small bundles. We measured the width of YVIFL fibers in buffer, sampling from multiple fields to minimize the influence of variations in staining. We found that YVIFL fibers were approximately 8 nm wide in isolation (standard deviation (SD) = 1.8 nm, 194 measurements), and slightly narrower within the context of a bundle (5 nm, SD = 0.9 nm, 36 measurements).

The third Set I peptide, YVVFL, was an interesting case. In water, YVVFL formed crystalline aggregates that were visible to the naked eye (the only peptide to do so in either solvent). However, TEM grids prepared from this sample showed only amorphous aggregates and rare, poorly defined fibrillar aggregates (Figure 1E). A separate preparation of YVVFL in water, incubated without shaking, showed abundant, short fibers (Supporting Information Figure S1). Measurements revealed that these fibers were approximately the same width as nonbundled YVIFL fibers (7 nm, SD = 1.3 nm, 167 measurements). Together, these data indicate that YVVFL has a higher aggregation propensity in water than is represented in the TEM images. YVVFL also aggregated in buffer, forming abundant fibers with a "beaded" appearance (Figure 1F). The irregularity of these fibers made accurate width measurements difficult, but sampling from nonbeaded portions of the fibers yielded widths that were similar to widths of YVIFL fibers and to widths of YVVFL fibers in water (9 nm, SD = 1.8 nm, 112 measurements).

Overall, aggregation was lower in the Set II peptides. YVVVL formed rare aggregates of bundled fibers in buffer. Similarly, rare aggregates of YVVVL also formed in water; however, individual fibers within those aggregates could not be distinguished (Figure 1G,H). YVGVL showed little evidence of aggregation in either solvent, aside from some small amorphous aggregates (Figure 1I,J). The aggregation propensity of Set II peptides studied by TEM is similar to that of the YGGFL control, which does not form fibrils. Few amorphous aggregates are rarely detected (Figure 1K,L).

Ion-Mobility Mass Spectrometry (IM-MS) Reveals Differences in Oligomer Distributions between Set I

dx.doi.org/10.1021/jp502473s | J. Phys. Chem. B 2014, 118, 7247–7256

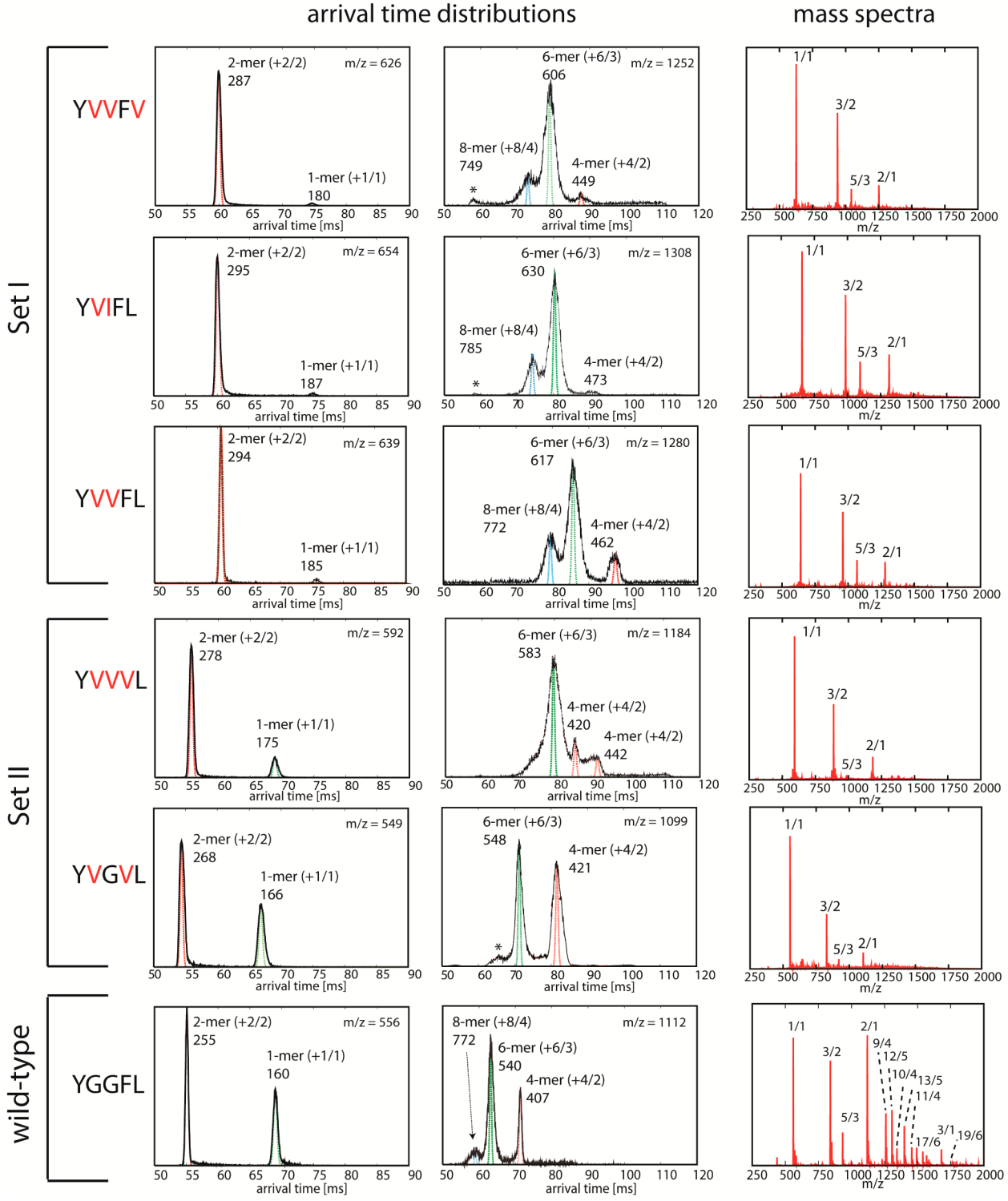

Figure 2. Representative ATDs at n/z = 1/1 (left) and 2/1 (middle) and mass spectra (right) of the five peptides and YGGFL control. ATDs containing multiple features are fitted with multiple Gaussians using intensity and arrival time as variables (Supporting Information section S2). Each feature is assigned with an oligomer to charge ratio (n/z) and its experimental cross section (σ, Å^2). In the mass spectra the peaks are annotated with n/z, where n is the oligomer number and z is the charge.

and Set II Peptides. The ESI-quadrupole mass spectra of the YGGFL mutants in water recorded on the high-resolution mobility instrument (Figure 2, right-hand column) show abundant formation of early transient oligomers. The peptides were sprayed at concentrations from 100 μM to 1 mM, and no significant changes were observed (data now shown). Peaks are annotated with their n/z ratios, where n is the oligomer number and z is the charge, indicating formation of n/z 1/1, n/z 3/2, n/z 5/3, and n/z 2/1. These four peaks are intense and observed in the mass spectra of all five peptide mutants. However, high m/z peaks are not observed in these mass spectra, as compared to the case for YGGFL, suggesting the structures, rather than

dx.doi.org/10.1021/jp502473s | J. Phys. Chem. B 2014, 118, 7247−7256

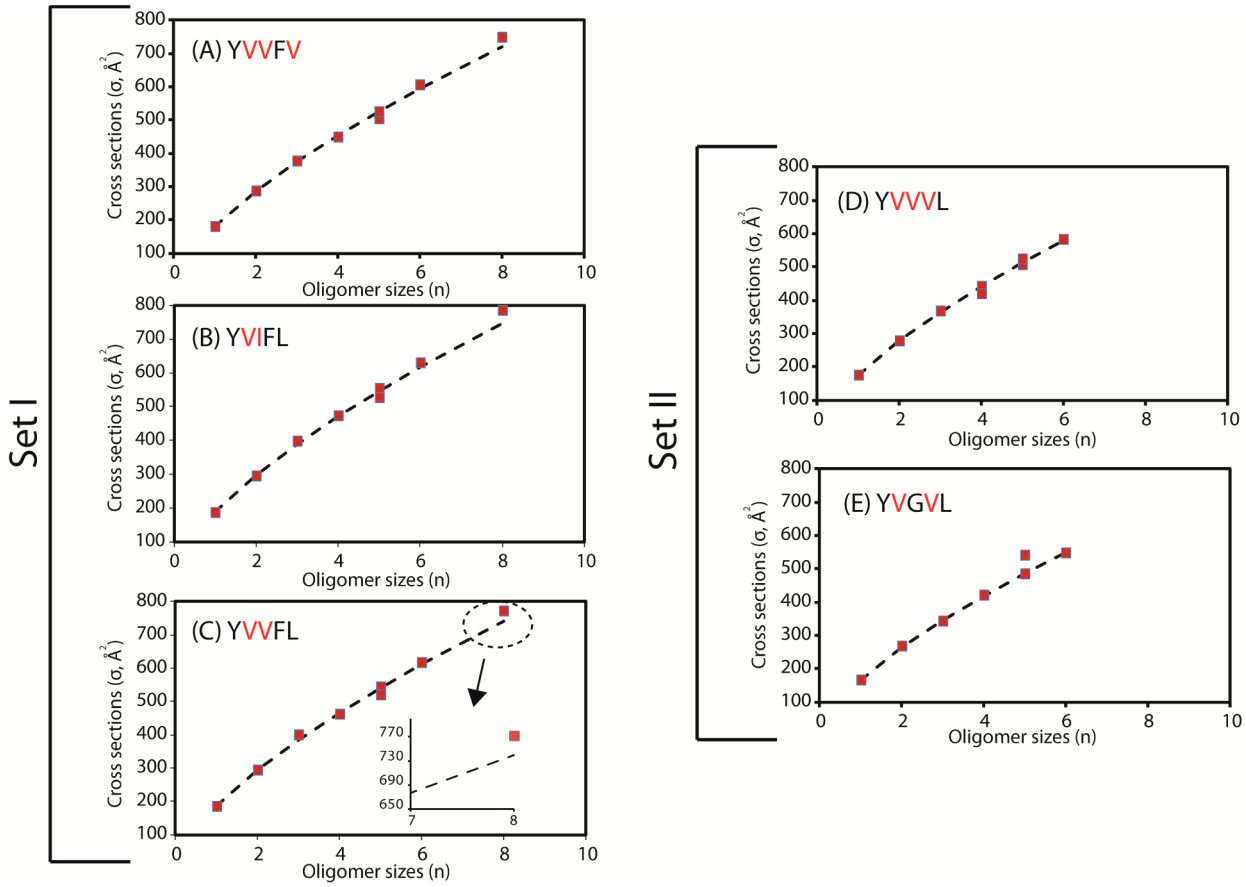

Figure 3. Experimental cross section σ as a function of oligomer size n *of the five mutants*. Isotropic cross sections[14] are shown in dashed lines.

populations of the oligomers determine fibril formation propensity. The features in the arrival time distributions (ATDs, Figure 2, first two columns) are assigned on the basis of the previous studies of YGGFL,[14] YAGFL,[42] and YVIFL under different pH conditions.[43] The peaks with n/z 1/1 have ATDs containing features of a dimer and a monomer for all peptides (Figure 2, left column). Although the dimer features appear to be dominant in all cases, Set II peptides have higher relative intensities for the monomer features than Set I. A recent study on dimerization of chirally mutated Enkephalin YAGFL[42] suggests that the relative intensities of monomer and dimer features in ATDs are well-correlated to the tendency for stable oligomer formation, and the subsequent aggregation propensity of a peptide. Hence, Set I peptides are predicted to have a greater tendency to aggregate than Set II peptides.

The n/z 3/2 ATDs have only a single narrow feature for each peptide system, strongly suggesting only a single conformer for each peptide system (Supporting Information Figure S3, left panel). On the other hand, the n/z 5/3 ATDs exhibit at least two different features (Supporting Information Figure S3, right panel), a compact pentamer, which is consistent with our previous study on YVIFL at high pH values and the isotropic model,[14,43] and a somewhat more extended feature. For YVGVL, the two features are well-resolved with the longer time ATD feature for n/z 5/3 ATD of YVGVL significantly larger than isotropic (σ = 541 Å^2), indicating the YVGVL pentamer can adopt an extended conformation. A possible explanation for this nonisotropic structure will be given in the T-REMD modeling section.

The mass spectral peaks with n/z 2/1 have ATDs showing multiple oligomer features consisting of a tetramer, a hexamer, and an octamer in the case of Set I peptides (Figure 2, right ATD panels). From this data, it is interesting to observe that the overall oligomer distributions for Set I peptides are very similar, with the largest oligomer being an octamer. For Set II peptides, tetramers and hexamers are abundant, but no larger oligomers are significantly populated. The features at 56−57 ms in the ATDs of YVVFV and YVIFL, and 64 ms in YVGVL appear to correspond to larger oligomers; however the intensities of the features are not high. The IM-MS data thus suggests that Set I peptides have higher propensities to form high-order structures than Set II.

In Figure 3, the experimental cross sections are compared to the isotropic model computed from the experimental monomer cross sections.[14] The octamer of all three Set I peptides shows a clear (~5%) positive deviation from the isotropic model (see the inset in Figure 3C of the YVVFL data), suggesting a transition may be occurring at the octamer to β-sheet containing oligomers, as previously observed for other peptide systems[14,25,43,44] and supported by the TEM and X-ray data presented here.

T-REMD Simulations Suggest High Aggregation Propensities of Set I Peptides. A previous study on YVIFL under different pH conditions shows that structural differences at the tetramer level correlate well with experimental aggregation propensity.[43] The tetramers are also populated in all peptides studied here. T-REMD simulations of the tetramers indicate the mutant oligomers adopt more β-rich character than the wild-type (wt), as shown by the Define Secondary Structure

dx.doi.org/10.1021/jp502473s | J. Phys. Chem. B 2014, 118, 7247−7256

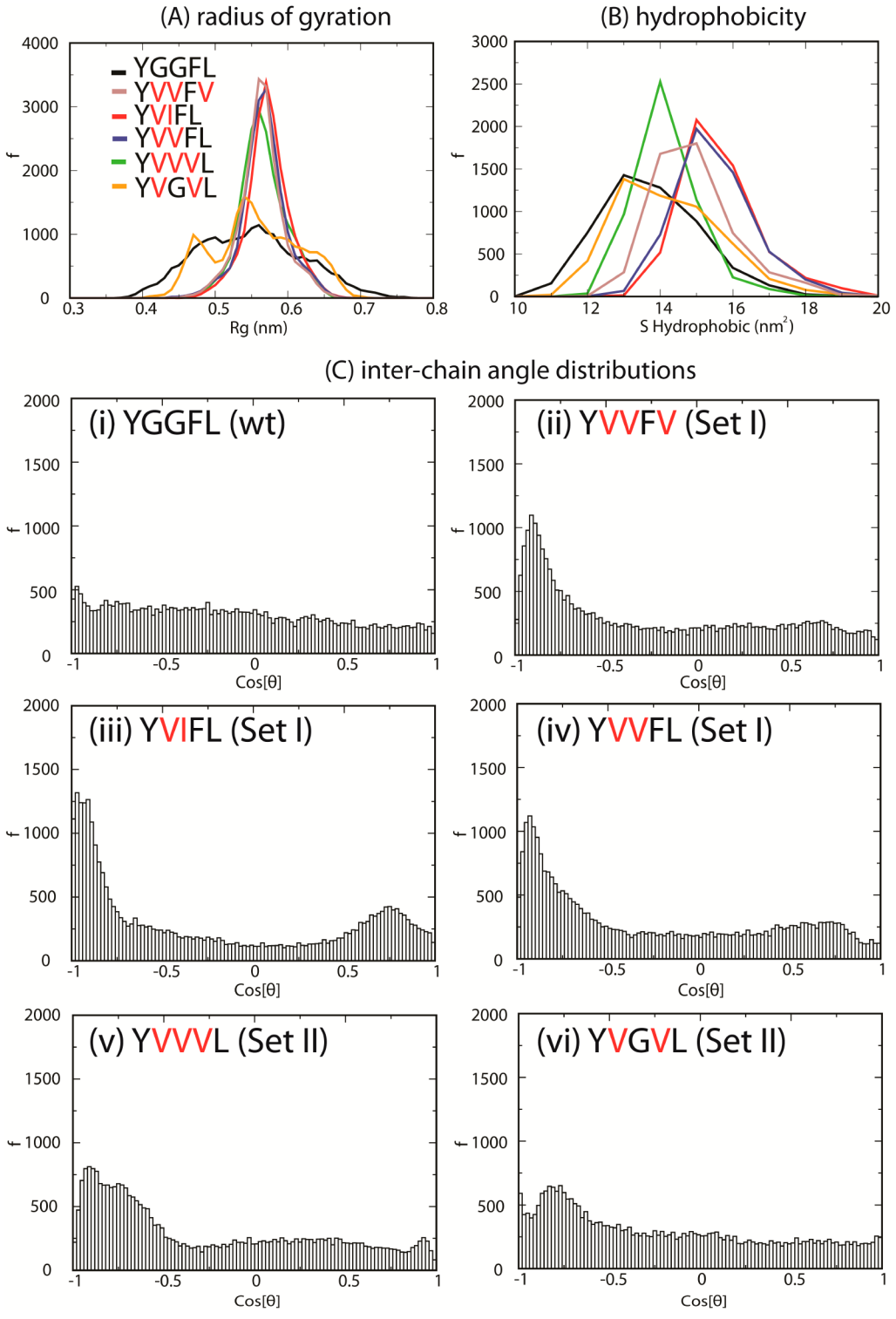

Figure 4. (A) Radius of gyration (R_g) of the monomer chain extracted from tetramers, (B) hydrophobic solvent accessible surface area (HSASA), and (C) interchain angle distributions of the tetramers obtained from T-REMD simulations.

of Proteins (DSSP) analysis[45] (Supporting Information Figure S2), although random coil is still dominant. However, previous studies have shown that secondary structural content *per se* is not a good indicator of aggregation propensity.[25,43] Knowledge of aggregation-prone conformations,[14] as well as specific conformations adopted predominantly by individual peptide chains within the oligomers offer better insight into aggregation behavior.[25,44,46] The radius of gyration (Rg) of the monomeric chains extracted from the T-REMD tetramer trajectories at 300 K are given in Figure 4A. YVGVL shows a similar Rg distribution to the wt with both compact and elongated conformations, whereas the remaining four peptides have a single distribution with the Rg values centered near 0.57 nm. The presence of hydrophobic valine, leucine and isoleucine can increase hydrophobic solvent-accessible surface area (HSASA, Figure 4B) per residue and subsequently promote steric zipper

dx.doi.org/10.1021/jp502473s | J. Phys. Chem. B 2014, 118, 7247−7256

formation through hydrophobic interactions upon association as the oligomers grow in size.[46] This metric divides the wt and the five mutants into three groups: (1) the wt and YVGVL have the lowest HSASA, (2) YVVVL and YVVFV have medium HSASA and (3) the YVVFL and YVIFL have the highest HSASA. The analysis strongly correlates with relative aggregation propensity among the peptides observed by TEM.

A more detailed analysis of interchain angle distributions (Figure 4C) reveals differences in the aggregation properties of the tetramers. The angles are computed for the vectors defined by the Cα atoms of the second and fourth residues of each peptide chain. An ideal antiparallel β-sheet tetramer should have two-thirds of the angles with $\cos[\theta] = -1$ and the remaining with $\cos[\theta] = +1$, although the twisting of the β-sheet can shift the angles a few degrees.[47] YGGFL chains within the wt tetramer do not show any specific angle preference (Figure 4C-i), and the dominant population of angles for Set II peptides is shifted away from $\cos[\theta] = -1$ (Figure 4C-v,-vi). These data suggest that β-sheet tetramers are not a favored motif in these three peptide oligomers. In YGGFL, the majority of structures are unordered or isotropic.

The three most populated tetramer clusters of YGGFL and the five mutants are given in Figure 5. Glycine is the most

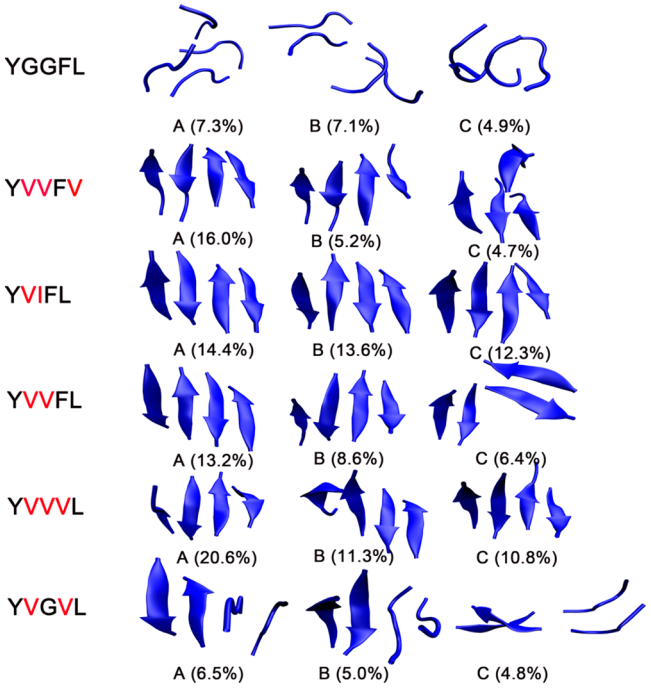

Figure 5. Representative structures of the three most populated clusters obtained from T-REMD simulations. The cutoff values from clustering are 0.3−0.4 nm on backbone atoms using the Daura algorithm.

flexible residue and mutating in bulkier residues tends to make the monomers less flexible.[42,48] In terms of β-turn flexibility YGGFL > Set II > Set I. This factor is evident in the structures of the peptides in Figure 5, where YGGFL is the most disordered, YVGVL the next most disordered and so on. Among the ordered tetramers, it is interesting that the only aggregation-prone structures observed in the simulations are single layer antiparallel β-sheets. Although the presence of these structures is consistent with eventual fibril formation, they suggest that the kinetics will be relatively slower than systems with mixed parallel/antiparallel β-sheets due to the entropic effect.[43,49] The absence of steric zippers is also consistent with relatively slower fibril formation kinetics.[43]

For YVVVL, distorted antiparallel β-sheets are observed (Figure 5) in addition to unordered structures, which is consistent with the inability of this peptide to from fibrils. For YVGVL, a similar structural content is found for the tetramers. However, its top three clusters contain an interesting class of structures in which two antiparallel dimers interact through terminal salt-bridges and tyrosine π-stacking to form a relatively stable, extended tetramer (Figure 5 structure C). This type of structure can be stable due to the low hydrophobicity of the peptide preventing collapse into more compact structures (Supporting Information Figure S2). The average cross section of these structures is 482 Å^2. The cross section of an extended pentamer containing this structure motif can be estimated to be 559 Å^2 on the basis of the isotropic equation,[14] providing an explanation for the observed extended pentamer of this peptide (541 Å^2 vs 485 Å^2 for the compact pentamer, Figure 3). It is not clear why the extended tetramer is not experimentally observed but perhaps it needs the additional monomer to fully stabilize the structure.

The Set I peptides (Figure 4C-ii,-iii,-iv) show a major distribution near $\cos[\theta] = -0.9$ (antiparallel) and a small population (which is clearly visible for YVIFL) at $\cos[\theta] = +0.8$ (parallel). Thus, these peptides are better than Set II peptides at forming antiparallel β-sheet tetramers, with YVIFL adopting the most ideal configuration, followed by YVVFL and YVVFV.

X-ray Crystallography Reveals the Differences in β-Sheet Packing Responsible for Fibril Formation Kinetics. As discussed in previous sections, Set I peptides have similar oligomerization mechanisms but different fibril formation kinetics and aggregate morphologies. A previous study of NH_2-Ile-Phe-COOH and NH_2-Val-Phe-COOH dipeptides indicate that the Ile-Phe dipeptide can aggregate into fibrils with structures similar to the nanotubes of diphenylalanine peptide (NH_2-Phe-Phe-COOH), whereas Val-Phe is much less effective.[50] Thus, the differences between YVIFL and YVVFL (or YVVFV) may well originate from the difference between Ile-Phe and Val-Phe hydrophobic pairs. However, unlike the previous work showing NH_2-Val-Phe-COOH cannot aggregate, we show that YVVFL can form well-defined fibrils whereas YVVFV is much less effective. X-ray crystallography can be used to visualize the packing structures of peptide chains within a crystal lattice and identify factors corresponding to differences in aggregation propensity. Hence we applied this method to YVVFV and YVVFL to see if differences in structure are found.

The YVVFV crystal structure shows antiparallel β-strands stacked via main chain hydrogen bonding to form a pair-of-sheets steric zipper (Figure 6A). The two sheets are weakly bound to each other via *face to back* interactions involving either hydrophobic interactions between valine 2 and valine 5 (Figure 6A, panels a,b,c) or π-stacking between opposing stacks of tyrosine 1 and phenylalanine 4 (Supporting Information Figure S4). Both interfaces nonetheless have a large solvent exposed area. Like YVVFV, the YVVFL crystal structure also shows antiparallel β-strands stacked *face to back* via main chain hydrogen bonding (Figure 6B). However, here the two β-sheets of this steric zipper run antiparallel to each other, unlike YVVFV where the mating sheets are parallel. The two YVVFL stacks interact with each other more strongly than in YVVFV, in part due to the hydrophobic interface between tyrosine 1, valine 3 and phenylalanine 4 (Figure 6B, panels a,b,c). The

dx.doi.org/10.1021/jp502473s | J. Phys. Chem. B 2014, 118, 7247−7256

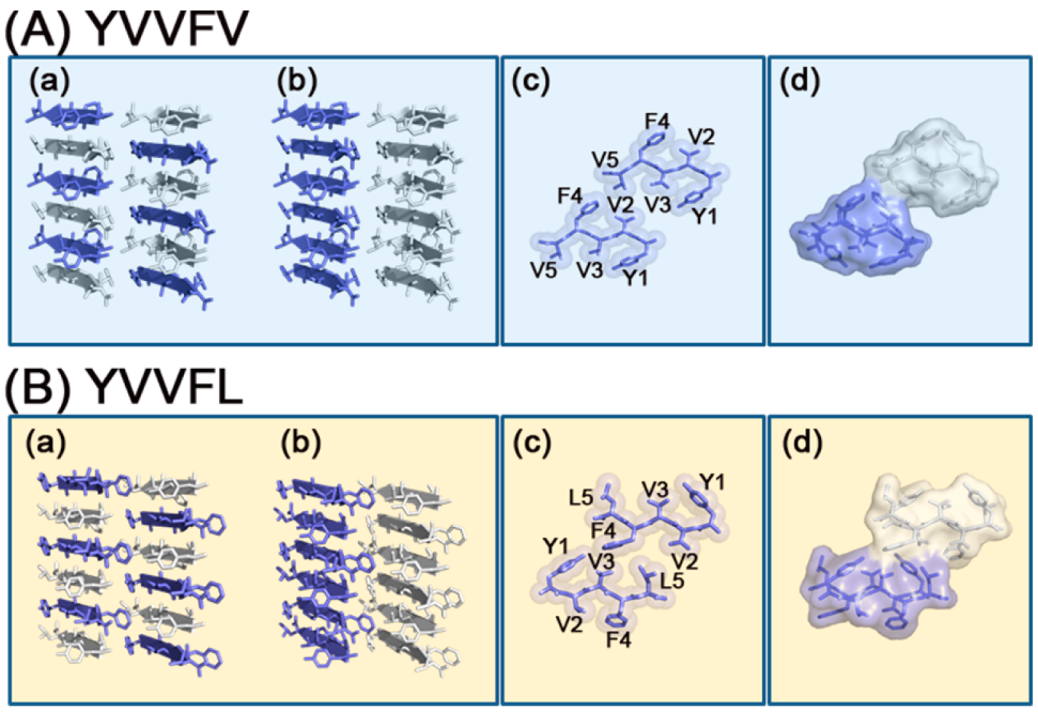

Figure 6. (A) (a, b) Sheet architecture of YVVFV. The strands are antiparallel to each other within one sheet and parallel between two mating sheets. (c) Dry interface. (d) Buried surface area. (B) (a, b) Sheet architecture of YVVFL. The strands are antiparallel to each other within one sheet and also between two mating sheets. (c) Dry interface. (d) Buried surface area.

outside surface is covered by a large number of water molecules.

For both YVVFV and YVVFL structures, only the odd numbered residues within one sheet face inward and two mating sheets are related to each other by translation. Both types of face to back interactions found in YVVFV and YVVFL are classified as Class 6 steric zipper according to Sawaya et al.[51]

The shape complementarity, a measure of stability, is slightly higher for YVVFL (0.73 vs 0.69) and the buried surface area (286 Å^2, Figure 6B, panel d) is double that of YVVFV (143 Å^2, Figure 6A, panel d). This result is consistent with T-REMD simulations, which predict that a single layer β-sheet of YVVFL has more hydrophobic surface area than YVVFV; thus, when a YVVFL steric zipper is formed, the buried hydrophobic surface should also be larger. The atomic resolution structures of YVVFL and YVVFV are in agreement with the TEM data showing the former makes abundant fibrils whereas the latter makes only amorphous aggregates and rare bundles of fibers.

SUMMARY AND CONCLUSIONS

Starting from a nonaggregating peptide YGGFL, we made amino acid substitutions to enhance hydrophobicity and obtain two sets of mutants. The first set of YVVFV, YVIFL, and YVVFL form structurally similar oligomers (n = 1−8) but have varied fibril formation propensities (i.e., YVIFL > YVVFL ≫ YVVFV) and morphologies. Comparing YVVFL and YVVFV, we find that atomic resolution X-ray structures suggest there are stronger interactions at the dry interfaces of YVVFL as compared to the inerfaces of YVVFV. These two peptides are the first and also the smallest aggregating systems (pentapeptide) with solved X-ray antiparallel face to back steric zipper structures. Although being in the same symmetry class, the pairs of strands in contact between sheets have a parallel orientation in YVVFL and antiparallel in YVVFV. The last two mutants, YVVVL and YVGVL, form only rare bundles of fibers or amorphous aggregates, respectively. In these two systems, the loss of the phenylalanine residue in position 4 completely suppresses the formation of oligomers larger than a hexamer. YVVVL can form some β-sheet structures according to the simulation, but the interactions at the dry interface between pairs of sheets are expected to be much weaker than for Set I peptides. Our findings lead to two conclusions:

- Early oligomer conformations play an important role in determining the possible protofibril structures that a peptide system can access (i.e., single β-sheet or double-sheet steric zipper). However, we find the stabilities of those structures are highly residue-dependent: isoleucine > leucine ≫ valine. This finding contrasts with the PASTA algorithm that indicates valine is the dominant non aromatic aggregation prone residue. Phenylalanine has a profound impact on aggregation propensity, especially when located next to another hydrophobic residue.
- Only the systems with significant interactions between pairs of β-sheets and steric zippers can form fibrils. This suggests that among different classes of steric zippers,[51,52] some may have a stronger tendency to self-assemble into nanostructures than the others. Within the same class, interactions between mating sheets that lead to high shape complementarity and buried surface area will enhance aggregation kinetics.

ASSOCIATED CONTENT

Supporting Information

Full description of the simulation protocol, DSSP analysis, ion-mobility mass spectrometry; related figures; and crystal data. This material is available free of charge via the Internet at http://pubs.acs.org.

dx.doi.org/10.1021/jp502473s | J. Phys. Chem. B 2014, 118, 7247−7256

Accession Codes

The coordinates of the YVVFL and YVVFV crystal structures have been deposited in the Protein Data Bank, www.pdb.org (PDB ID 4ONK and 4OLR).

AUTHOR INFORMATION

Corresponding Author

*M. T. Bowers. E-mail: bowers@chem.ucsb.edu. Tel: +1-805-893-2673.

Author Contributions

⊥T.D.D., N.E.L., and S.S. contributed equally. All authors conceived and designed the experiments. T.D.D. performed the IM-MS experiments and T-REMD simulations. N.E.L. did the TEM measurements. S.S. and M.R.S. grew the X-ray crystals and analyzed the crystallographic data. T.D.D. and M.T.B. co-wrote the paper.

Notes

The authors declare no competing financial interest.

ACKNOWLEDGMENTS

The authors thank Ms. Margaret Condron for synthesizing the peptides. T.D.D. thanks Nicholas Economou, Breanna Johnson, and Dr. Christian Bleiholder for useful discussion. We thank Michael Collazo at the UCLA crystallization facility for setting up robot screens and K. Rajashankar and beamline staff at Argonne Photon Source, Northeastern Collaborative Access Team beamlines 24-ID-E, for data collection. We gratefully acknowledge support from the National Science Foundation grants CHE-1301032 (M.T.B.) and MCB-0958111 (D.S.E.), and the National Institutes of Health grants 1RO1AG047116-01 (M.T.B.), NS038328 (D.B.T.), AG041295 (D.B.T.), and by the Jim Easton Consortium for Drug Discovery and Biomarkers at UCLA (D.B.T.). This work used the Extreme Science and Engineering Discovery Environment (XSEDE), which is supported by National Science Foundation grant number OCI-1053575. The authors acknowledge the Texas Advanced Computing Center (TACC) at The University of Texas at Austin for providing HPC resources through the XSEDE grant number TG-CHE130004 (M.T.B.). We acknowledge support from the Center for Scientific Computing at the CNSI and MRL: an NSF MRSEC (DMR- 1121053) and NSF CNS-0960316. We also acknowledge the use of the NRI-MCDB Microscopy Facility at UC, Santa Barbara.

REFERENCES

(1) Chiti, F.; Dobson, C. M. Protein Misfolding, Functional Amyloid, and Human Disease. *Annu. Rev. Biochem.* **2006**, *75*, 333−366.

(2) Eisenberg, D.; Nelson, R.; Sawaya, M. R.; Balbirnie, M.; Sambashivan, S.; Ivanova, M. I.; Madsen, A. O.; Riekel, C. The Structural Biology of Protein Aggregation Diseases: Fundamental Questions and Some Answers. *Acc. Chem. Res.* **2006**, *39*, 568−575.

(3) O'Brien, R. J.; Wong, P. C. Amyloid Precursor Protein Processing and Alzheimer's Disease. *Annu. Rev. Neurosci.* **2011**, *34*, 185−204.

(4) West, M. W.; Wang, W.; Patterson, J.; Mancias, J. D.; Beasley, J. R.; Hecht, M. H. De Novo Amyloid Proteins from Designed Combinatorial Libraries. *Proc. Natl. Acad. Sci. U. S. A.* **1999**, *96*, 11211−11216.

(5) Laganowsky, A.; Liu, C.; Sawaya, M. R.; Whitelegge, J. P.; Park, J.; Zhao, M. L.; Pensalfini, A.; Soriaga, A. B.; Landau, M.; Teng, P. K.; et al. Atomic View of a Toxic Amyloid Small Oligomer. *Science* **2012**, *335*, 1228−1231.

(6) Apostol, M. I.; Perry, K.; Surewicz, W. K. Crystal Structure of Human Prion Protein Fragment Reveals a Motif for Oligomer Formation. *J. Am. Chem. Soc.* **2013**, *135*, 10202−10205.

(7) Liu, C.; Zhao, M.; Jiang, L.; Cheng, P. N.; Park, J.; Sawaya, M. R.; Pensalfini, A.; Gou, D.; Berk, A. J.; Glabe, C. G.; et al. Out-of-Register β-Sheets Suggest a Pathway to Toxic Amyloid Aggregates. *Proc. Natl. Acad. Sci. U. S. A.* **2012**, *109*, 20913−20918.

(8) Lin, H.; Bhatia, R.; Lal, R. Amyloid-β Protein Forms Ion Channels: Implications for Alzheimer's Disease Pathophysiology. *FASEB J.* **2001**, *15*, 2433−2444.

(9) Quist, A.; Doudevski, I.; Lin, H.; Azimova, R.; Ng, D.; Frangione, B.; Kagan, B.; Ghiso, J.; Lal, R. Amyloid Ion Channels: A Common Structural Link for Protein-Misfolding Disease. *Proc. Natl. Acad. Sci. U. S. A.* **2005**, *102*, 10427−10432.

(10) Diaz-Avalos, R.; Long, C.; Fontano, E.; Balbirnie, M.; Grothe, R.; Eisenberg, D.; Caspar, D. L. D. Cross-β Order and Diversity in Nanocrystals of an Amyloid-Forming Peptide. *J. Mol. Biol.* **2003**, *330*, 1165−1175.

(11) Nelson, R.; Eisenberg, D. Recent Atomic Models of Amyloid Fibril Structure. *Curr. Opin. Struc. Biol.* **2006**, *16*, 260−265.

(12) Kajava, A. V.; Baxa, U.; Steven, A. C. β-Arcades: Recurring Motifs in Naturally Occurring and Disease-Related Amyloid Fibrils. *FASEB J.* **2010**, *24*, 1311−1319.

(13) Li, W. K.; Lee, V. M. Y. Characterization of Two VQIXXK Motifs for Tau Fibrillization in Vitro. *Biochemistry* **2006**, *45*, 15692−15701.

(14) Bleiholder, C.; Dupuis, N. F.; Wyttenbach, T.; Bowers, M. T. Ion Mobility-Mass Spectrometry Reveals a Conformational Conversion from Random Assembly to β-Sheet in Amyloid Fibril Formation. *Nat. Chem.* **2011**, *3*, 172−177.

(15) Sakai, H.; Watanabe, K.; Asanomi, Y.; Kobayashi, Y.; Chuman, Y.; Shi, L.; Masuda, T.; Wyttenbach, T.; Bowers, M. T.; Uosaki, K.; et al. Formation of Functionalized Nanowires by Control of Self-Assembly Using Multiple Modified Amyloid Peptides. *Adv. Funct. Mater.* **2013**, *23*, 4881−4887.

(16) Adler-Abramovich, L.; Reches, M.; Sedman, V. L.; Allen, S.; Tendler, S. J. B.; Gazit, E. Thermal and Chemical Stability of Diphenylalanine Peptide Nanotubes: Implications for Nanotechnological Applications. *Langmuir* **2006**, *22*, 1313−1320.

(17) Hartgerink, J. D.; Beniash, E.; Stupp, S. I. Self-Assembly and Mineralization of Peptide-Amphiphile Nanofibers. *Science* **2001**, *294*, 1684−1688.

(18) Ghadiri, M. R.; Granja, J. R.; Milligan, R. A.; Mcree, D. E.; Khazanovich, N. Self-Assembling Organic Nanotubes Based on a Cyclic Peptide Architecture. *Nature* **1994**, *372*, 709−709.

(19) Olzscha, H.; Schermann, S. M.; Woerner, A. C.; Pinkert, S.; Hecht, M. H.; Tartaglia, G. G.; Vendruscolo, M.; Hayer-Hartl, M.; Hartl, F. U.; Vabulas, R. M. Amyloid-Like Aggregates Sequester Numerous Metastable Proteins with Essential Cellular Functions. *Cell* **2011**, *144*, 67−78.

(20) de la Paz, M. L.; Goldie, K.; Zurdo, J.; Lacroix, E.; Dobson, C. M.; Hoenger, A.; Serrano, L. De Novo Designed Peptide-Based Amyloid Fibrils. *Proc. Natl. Acad. Sci. U. S. A.* **2002**, *99*, 16052−16057.

(21) Nagarkar, R. P.; Hule, R. A.; Pochan, D. J.; Schneider, J. P. De Novo Design of Strand-Swapped β-Hairpin Hydrogels. *J. Am. Chem. Soc.* **2008**, *130*, 4466−4474.

(22) Smith, G. D.; Griffin, J. F. Conformation of [Leu5]Enkephalin from X-Ray-Diffraction - Features Important for Recognition at Opiate Receptor. *Science* **1978**, *199*, 1214−1216.

(23) Trovato, A.; Chiti, F.; Maritan, A.; Seno, F. Insight into the Structure of Amyloid Fibrils from the Analysis of Globular Proteins. *PLoS Comput. Biol.* **2006**, *2*, 1608−1618.

(24) Trovato, A.; Seno, F.; Tosatto, S. C. E. The PASTA Server for Protein Aggregation Prediction. *Protein Eng. Des. Sel.* **2007**, *20*, 521−523.

(25) Do, T. D.; Economou, N. J.; LaPointe, N. E.; Kincannon, W. M.; Bleiholder, C.; Feinstein, S. C.; Teplow, D. B.; Buratto, S. K.; Bowers, M. T. Factors That Drive Peptide Assembly and Fibril Formation: Experimental and Theoretical Analysis of Sup35 NNQQNY Mutants. *J. Phys. Chem. B* **2013**, *117*, 8436−8446.

(26) Wyttenbach, T.; Bowers, M. T. Structural Stability from Solution to the Gas Phase: Native Solution Structure of Ubiquitin

Survives Analysis in a Solvent-Free Ion Mobility-Mass Spectrometry Environment. *J. Phys. Chem. B* **2011**, *115*, 12266−12275.
(27) Mason, E. A. *Transport Properties of Ions in Gases*, 99 ed.; John Wiley & Sons: New York, 1988.
(28) Gidden, J.; Ferzoco, A.; Baker, E. S.; Bowers, M. T. Duplex Formation and the Onset of Helicity in Poly D(cG)$_n$ Oligonucleotides in a Solvent-Free Environment. *J. Am. Chem. Soc.* **2004**, *126*, 15132−15140.
(29) Kemper, P. R.; Dupuis, N. F.; Bowers, M. T. A New, Higher Resolution, Ion Mobility Mass Spectrometer. *Int. J. Mass. Spectrom.* **2009**, *287*, 46−57.
(30) Sugita, Y.; Okamoto, Y. Replica-Exchange Molecular Dynamics Method for Protein Folding. *Chem. Phys. Lett.* **1999**, *314*, 141−151.
(31) Hess, B.; Kutzner, C.; Spoel, D. v. d.; Lindahl, E. Gromacs 4: Algorithms for Highly Efficient, Load-Balanced, and Scalable Molecular Simulation. *J. Chem. Theory Comput.* **2008**, *4*, 435−437.
(32) Spoel, D. V. D.; Lindahl, E.; Hess, B.; Groenhof, G.; Mark, A. E.; Berendsen, H. J. C. Gromacs: Fast, Flexible, and Free. *J. Comput. Chem.* **2005**, *26*, 1701−1718.
(33) Damm, W.; Halgren, T. A.; Murphy, R. B.; Smondyrev, A. M.; Friesner, R. A.; Jorgensen, W. L. OPLS_2002: A New Version of the OPLS-AA Force Field. *Abstr. Pap. Am. Chem. S.* **2002**, *224*, U471−U471.
(34) Jorgensen, W. L.; Maxwell, D. S.; TiradoRives, J. Development and Testing of the OPLS All-Atom Force Field on Conformational Energetics and Properties of Organic Liquids. *J. Am. Chem. Soc.* **1996**, *118*, 11225−11236.
(35) Jorgensen, W. L.; Chandrasekhar, J.; Madura, J. D.; Impey, R. W.; Klein, M. L. Comparison of Simple Potential Functions for Simulating Liquid Water. *J. Chem. Phys.* **1983**, *79*, 926−935.
(36) Daura, X.; Gademann, K.; Jaun, B.; Seebach, D.; Gunsteren, W. F. v.; Mark, A. E. Peptide Folding: When Simulation Meets Experiment. *Angew. Chem., Int. Ed.* **1999**, *38*, 236−240.
(37) Kabsch, W. Automatic Processing of Rotation Diffraction Data from Crystals of Initially Unknown Symmetry and Cell Constants. *J. Appl. Crystallogr.* **1993**, *26*, 795−800.
(38) Read, R. J. Pushing the Boundaries of Molecular Replacement with Maximum Likelihood. *Acta Crystallogr. D* **2001**, *57*, 1373−1382.
(39) Otwinowski, Z.; Minor, W. Processing of X-Ray Diffraction Data Collected in Oscillation Mode. *Methods Enzymol.* **1997**, *276*, 307−326.
(40) Emsley, P.; Cowtan, K. Coot: Model-Building Tools for Molecular Graphics. *Acta Crystallogr. D* **2004**, *60*, 2126−2132.
(41) Adams, P. D.; Afonine, P. V.; Bunkoczi, G.; Chen, V. B.; Davis, I. W.; Echols, N.; Headd, J. J.; Hung, L. W.; Kapral, G. J.; Grosse-Kunstleve, R. W.; et al. Phenix: A Comprehensive Python-Based System for Macromolecular Structure Solution. *Acta Crystallogr. D* **2010**, *66*, 213−221.
(42) Bleiholder, C.; Dupuis, N. F.; Bowers, M. T. Dimerization of Chirally Mutated Enkephalin Neurotransmitters: Implications for Peptide and Protein Aggregation Mechanisms. *J. Phys. Chem. B* **2013**, *117*, 1770−1779.
(43) Do, T. D.; Lapointe, N. E.; Economou, N. J.; Buratto, S. K.; Feinstein, S. C.; Shea, J. E.; Bowers, M. T. Effects of pH and Charge State on Peptide Assembly: The YVIFL Model System. *J. Phys. Chem. B* **2013**, *117*, 10759−10768.
(44) Bleiholder, C.; Do, T. D.; Wu, C.; Economou, N. J.; Bernstein, S. S.; Buratto, S. K.; Shea, J.-E.; Bowers, M. T. Ion Mobility Spectrometry Reveals the Mechanism of Amyloid Formation of Aβ(25−35) and Its Modulation by Inhibitors at the Molecular Level: Epigallocatechin Gallate and Scyllo-Inositol. *J. Am. Chem. Soc.* **2013**, *135*, 16926−16937.
(45) Joosten, R. P.; Beek, T. A. H. T.; Krieger, E.; Hekkelman, M. L.; Hooft, R. W. W.; Schneider, R.; Sander, C.; Vriend, G. A Series of PDB Related Databases for Everyday Needs. *Nucleic Acids Res.* **2011**, *39*, D411−D419.
(46) Lin, E. I.; Shell, M. S. Can Peptide Folding Simulations Provide Predictive Information for Aggregation Propensity? *J. Phys. Chem. B* **2010**, *114*, 11899−11908.
(47) Knowles, T. P. J.; De Simone, A.; Fitzpatrick, A. W.; Baldwin, A.; Meehan, S.; Rajah, L.; Vendruscolo, M.; Welland, M. E.; Dobson, C. M.; Terentjev, E. M., Twisting Transition between Crystalline and Fibrillar Phases of Aggregated Peptides. *Phys. Rev. Lett.* **2012**, *109*.
(48) Smith, G. D.; Griffin, J. F. Conformation of [Leu5] Enkephalin from X-Ray Diffraction: Features Important for Recognition at Opiate Receptor. *Science* **1978**, *199*, 1214−1216.
(49) Jeon, J.; Shell, M. S. Charge Effects on the Fibril-Forming Peptide KTVIIE: A Two-Dimensional Replica Exchange Simulation Study. *Biophys. J.* **2012**, *102*, 1952−1960.
(50) de Groot, N. S.; Parella, T.; Aviles, F. X.; Vendrell, J.; Ventura, S. Ile-Phe Dipeptide Self-Assembly: Clues to Amyloid Formation. *Biophys. J.* **2007**, *92*, 1732−1741.
(51) Sawaya, M. R.; Sambashivan, S.; Nelson, R.; Ivanova, M. I.; Sievers, S. A.; Apostol, M. I.; Thompson, M. J.; Balbirnie, M.; Wiltzius, J. J. W.; MacFarlane, H. T.; et al. Atomic Structures of Amyloid Cross-β Spines Reveal Varied Steric Zippers. *Nature* **2007**, *447*, 453−457.
(52) Nelson, R.; Sawaya, M. R.; Balbirnie, M.; Madsen, A. O.; Riekel, C.; Grothe, R.; Eisenberg, D. Structure of the Cross-β Spine of Amyloid-Like Fibrils. *Nature* **2005**, *435*, 773−778.